

Contents lists available at ScienceDirect

Acta Materialia

journal homepage: www.elsevier.com/locate/actamat



Full length article

Post-uniform elongation and tensile fracture mechanisms of Fe-18Mn-0.6C-xAl twinning-induced plasticity steels



Ha-Young Yu ^a, Sang-Min Lee ^a, Jae-Hoon Nam ^a, Seung-Joon Lee ^{a, b}, Damien Fabrègue ^c, Myeong-heom Park ^d, Nobuhiro Tsuji ^d, Young-Kook Lee ^{a, *}

- ^a Department of Materials Science and Engineering, Yonsei University, Seoul, 03722, Republic of Korea
- ^b Current affiliation: Joining and Welding Research Institute, Osaka University, Osaka, 567-0047, Japan
- ^c Université de Lyon, CNRS, F-669621, Villeurbanne, France
- ^d Department of Materials Science and Engineering, Kyoto University, Kyoto, 606-8501, Japan

ARTICLE INFO

Article history: Received 8 February 2017 Received in revised form 4 April 2017 Accepted 6 April 2017 Available online 6 April 2017

Keywords: Mechanical behavior Crack propagation Fracture mechanism Deformation twinning X-ray tomography

ABSTRACT

The objective of the present study was to elucidate the complicated interrelationship between necking, post-uniform elongation (epu), strain rate sensitivity (SRS), fracture mechanism and Al concentration in Fe-18Mn-0.6C-xAl twinning-induced plasticity steels. Many tensile tests were conducted for in- and exsitu observations of necking, fracture surfaces, crack propagation and the density and size of micro-voids with the assistance of a high-speed camera and X-ray tomographic equipment. The addition of Al increased epu, SRS and reduction ratios in dimension of the neck part of tensile specimens, and also changed fracture mode from quasi-cleavage to ductile fracture at the edge part. The quasi-cleavage surface of Al-free specimen was induced by edge and side cracks occurring along grain boundary junctions and twin boundaries within the edges and side surfaces where local deformation bands meet. The ductile-fracture surface of 1.5 %Al-added specimen was formed by the coalescence of micro-voids. While the side-to-middle crack propagation occurred in Al-free and 1 %Al-added specimens due to side cracks, the middle-to-side crack propagation was observed in 1.5 %Al-added specimen. The Al-free specimen had the larger size of the 20 largest voids compared to the 1.5 %Al-added specimen despite its lower void density and local strain due to the accelerated growth of voids near the tips of side cracks. Evaluating the negligible epu of Al-free specimen by SRS is not deemed to be reasonable due to its inappreciable necking and side cracks. The improvement of e_{pu} in 1.5 %Al-added specimen is primarily due to disappearance of edge and side cracks.

© 2017 Acta Materialia Inc. Published by Elsevier Ltd. All rights reserved.

1. Introduction

High manganese twinning-induced plasticity (TWIP) steel has attracted much attention due to its remarkable combination of high tensile stress (UTS) (>800 MPa) and high uniform elongation (e_u) (>60%), which is caused primarily by mechanical twinning occurring during plastic deformation [1–4]. However, Al-free TWIP steel possesses inappreciable post-uniform elongation (e_{pu}) [5], which is one of important parameters for the capability of hole expansion [6], although its e_{pu} is improved to some extent by the addition of Al [3]. Nevertheless, until now there are few articles on the behaviors of necking and e_{pu} of TWIP steels and on their dependencies of Al

* Corresponding author. E-mail address: yklee@yonsei.ac.kr (Y.-K. Lee). concentration. Only some of present authors [3] reported that the extremely low e_{pu} of Al-free C-bearing TWIP steel is most likely due to its negative strain rate sensitivity (SRS) and that the increase of e_{pu} in Al-added TWIP steel is attributed to the SRS improved by the addition of Al. This analysis was based on the previous results that negative SRS occurs due to dynamic strain aging (DSA) in Al-free C-bearing TWIP steel [3,7–11] and is improved by the addition of Al due to suppressed DSA [3,7], and that e_{pu} shows a proportionality to SRS in many materials [12].

However, besides a mechanical aspect of SRS, metallographic studies are necessary for better understanding of the behaviors of necking and e_{pu} in both Al-free and bearing TWIP steels. Thus, the present study restarted from the definition of e_{pu} : namely, because e_{pu} is non-uniform elongation from necking to failure in a stress vs. strain curve, e_{pu} strongly depends on when and how a tensile specimen fails. In other words, e_{pu} must be closely related to

necking and fracture mechanism. Considering the fracture behavior of TWIP steel in this viewpoint, Al-free TWIP steel with negligible epu abruptly fails almost without a narrowed neck of gauge portion during tensile deformation. This appears to indicate that the TWIP steel undergoes brittle fracture at least at the moment of failure, despite large eu. However, surprisingly the fracture surfaces of tensile specimens of TWIP steels are full of many fine dimples, a feature of ductile fracture generally accompanied by necking and epu, regardless of chemical compositions of steels and strain rate [3,7,8,13–17]. In spite of this controvertible fracture behavior of TWIP steel, it was reported that the fracture of TWIP steel occurs in association with the nucleation and coalescence of voids simply based on the SEM images of fracture surfaces showing many fine dimples [3,7,14,18–21].

In recent, Lorthios et al. [20] and Fabrègue et al. [19] observed the formation of micro-voids in Al-free Fe-22Mn-0.6C (wt.%) TWIP steel after and during tensile tests, respectively by means of X-ray microtomography. Lorthios et al. [20] detected large elliptical voids measuring >100 μm just below the shear fracture surface. However, the average volume fraction of voids near the fracture surface was ~0.06%, which was much lower than that (2%) of voids in dual-phase steel [22]. In addition, the large voids were rare and larger than dimples (<1 μm) observed in the fracture surface. Therefore, they reported that the primary large voids did not lead to final fracture, and fracture seems to be caused by the formation and early coalescence of secondary micro-voids. However, there is no explanation about when secondary micro-voids form and how their early coalescence occurs.

Fabrègue et al. [19] conducted *in-situ* observation of void formation with strain by means of X-ray microtomography. They found that the void densities of both Al-free austenitic TWIP steel and 316L austenitic stainless steel were even lower than those of Al alloys with the same *fcc* crystal structure; this matches well with the previous result reported by Lorthios et al. [20]. In addition, although 316L stainless steel possessed a higher void density at the significantly narrowed neck part of gauge portion compared to Alfree TWIP steel, it exhibited a higher e_{pu}. These X-ray microtomographic results cast a strong doubt that the nucleation and merging of voids are decisively responsible for the fracture of Al-free TWIP steel.

Accordingly, the fracture mechanisms of TWIP steels, even Alfree TWIP steel, are yet to be clear; as a result, it is more difficult to understand the variation of e_{pu} with the addition of Al. In addition, there is still neither quantitative analysis of necking nor a report on the relationship between fracture and Portevin—Le Chatelier (PLC) band observed in Al-free TWIP steel [8,23]. Therefore, the objective of the present study is to investigate the behaviors of necking, e_{pu} and fracture of TWIP steels with and without Al as comprehensively and quantitatively as possible in viewpoints of not only void formation but also PLC band propagation using various experimental techniques including X-ray microtomography.

2. Experimental procedure

2.1. Sample preparation

Three ~20-kg ingots of high manganese TWIP steels with different Al concentrations were made using a vacuum induction furnace. The actual chemical compositions of three steels are listed in Table 1. Hereafter, the TWIP steels are called OAI, 1AI and 1.5AI specimens, according to their Al concentrations. After solution-treated at 1100 °C for 2 h, the ingots were hot-rolled to ~6-mm thick plates at temperatures from ~1100 °C to 900 °C, and then water-quenched to room temperature. After surface descaling, the

Table 1
Chemical compositions of Fe-18Mn-0.6C-xAl TWIP steels used (wt %)

Steel	Mn	Al	С	Fe
OAl	17.65	0.02	0.62	Bal.
1Al	19.01	0.96	0.56	Bal.
1.5Al	17.48	1.42	0.58	Bal.

hot-rolled plates were cold-rolled from ~4-mm to ~1.5-mm thick sheets, corresponding to a thickness reduction of ~60%.

2.2. Tensile testing

Tensile tests were conducted for the following observations; necking, fracture surface, PLC band propagation, real-time crack propagation and void formation by means of *ex-situ* X-ray microtomography. All tensile specimens were made by wire electric discharge machining along the rolling direction from the coldrolled sheet, and their shape and size are shown in Fig. 1. The ASTM E8M-04 specimen (Fig. 1a) was used for the observation of necking and fracture surfaces. The small tensile specimen (Fig. 1b) was used for *in-situ* observation of the propagation of PLC bands and cracks. The tensile specimen for X-ray tomography is shown in Fig. 1c.

All tensile specimens were annealed at 1000 °C for 10 min under a vacuum atmosphere using a tube furnace, and then waterquenched to prevent carbide precipitation. The average grain sizes of annealed 0Al, 1Al and 1.5Al specimens were evaluated including annealing twins by the linear intercept method [24]; their values were ~35, 32 and 39 μ m, respectively. The annealed tensile specimens were strained at room temperature primarily at an initial strain rate ($\dot{\epsilon}$) of 1 × 10⁻³ s⁻¹. For the measurement of SRS, the annealed tensile specimens were deformed until failure with various $\dot{\epsilon}$ values ranging from 1 × 10⁻² s⁻¹ to 1 × 10⁻⁴ s⁻¹. Using the UTS values taken from the measured engineering stress-strain curves, a plot of ln UTS vs. In $\dot{\epsilon}$ was drawn. The relative SRS (m = dlnUTS/dln $\dot{\epsilon}$) [7] was obtained from the slope of the plot.

Tensile tests for observations of fracture surfaces and real-time cracking were carried out using a servo hydraulic universal tensile testing machine (Instron, 3382). Tensile tests for *ex-situ* observation of void formation were conducted using an Instron 5967 machine. For the *in-situ* observation of cracking, a low-magnification camera (Olympus, SZ61), which is operated at a frame rate of 30 frames/s (fps), was attached to the tensile machine. A high-speed camera (IX cameras, I-speed 221) with a frame rate of 10,500 fps was also utilized particularly for the 1.5Al specimen due

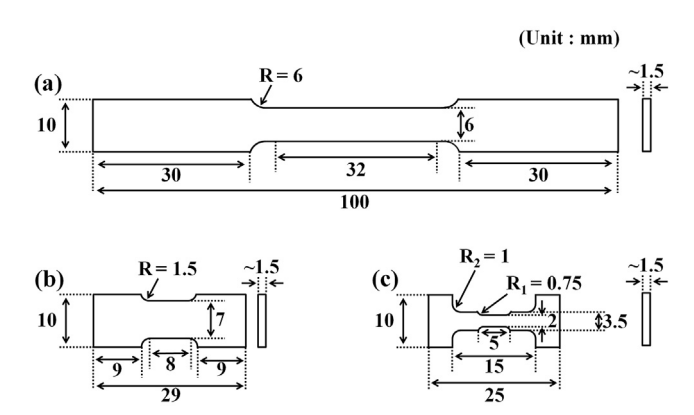


Fig. 1. Schematics of (a) ASTM 8M-04 tensile specimen, (b) tensile test specimen for *in-situ* observation of cracking and (c) tensile specimen for *ex-situ* X-ray tomography [19].

Download English Version:

https://daneshyari.com/en/article/5435870

Download Persian Version:

https://daneshyari.com/article/5435870

<u>Daneshyari.com</u>